



Cite this: *Phys. Chem. Chem. Phys.*,  
2024, 26, 12433

# A multi-FLP approach for CO<sub>2</sub> capture: investigating nitrogen, boron, phosphorus and aluminium doped nanographenes and the influence of a sodium cation†

Maxime Ferrer,<sup>ab</sup> Ibon Alkorta,<sup>ib</sup>\*<sup>a</sup> José Elguero<sup>a</sup> and Josep M. Oliva-Enrich<sup>c</sup>

The reactivity of B<sub>3</sub>N<sub>3</sub>-doped hexa-cata-hexabenzocoronene (B<sub>3</sub>N<sub>3</sub>-NG), Al<sub>3</sub>N<sub>3</sub>-NG, B<sub>3</sub>P<sub>3</sub>-NG and Al<sub>3</sub>P<sub>3</sub>-NG, models of doped nanographenes (NGs), towards carbon dioxide was studied with density functional theory (DFT) calculations at the M06-2X/6-311++G(3df,3pd)//M06-2X/6-31+G\* level of theory. The NG systems exhibit a poly-cyclic poly-frustrated Lewis pair (FLP) nature, featuring multiple Lewis acid/Lewis base pairs on their surface enabling the capture of several CO<sub>2</sub> molecules. The capture of CO<sub>2</sub> by these systems was investigated within two scenarios: (A) sequential capture of up to three CO<sub>2</sub> molecules and (B) capture of CO<sub>2</sub> molecules in the presence of a sodium cation. The resulting adducts were analyzed in terms of the activation barriers and relative stabilities. The presence of aluminium atoms changes the asynchrony of the reaction favoring the aluminium-oxygen bond and influences the regioselectivity of the multi-capture. A cooperative effect is predicted due to  $\pi$ -electron delocalization, with the sodium cation stabilizing the stationary points and favoring the addition of CO<sub>2</sub> to the NGs.

Received 2nd February 2024,  
Accepted 26th March 2024

DOI: 10.1039/d4cp00496e

rsc.li/pccp

## Introduction

Carbon dioxide (CO<sub>2</sub>) is a highly stable molecule commonly produced from the oxidation of mineral carbon or organic carbon chains. It is also a major greenhouse effect gas released as a result of human activities.<sup>1–3</sup> Various small molecules, including carbenes,<sup>4–9</sup> guanidines,<sup>10,11</sup> and phosphines,<sup>12–15</sup> have been studied for their ability to form adducts with CO<sub>2</sub>. However, the surplus production of CO<sub>2</sub> calls for more efforts to reduce its impact. For example, in 2022, the atmospheric CO<sub>2</sub> concentration reached an alarming new record, with an average yearly concentration of 417 ppm.<sup>16,17</sup>

The scientific community is heavily focused on searching for new techniques and methods to reduce the concentration of CO<sub>2</sub> in the atmosphere, and the main technologies being developed for its trapping can be categorized into three groups: absorption, adsorption, and membrane technologies.<sup>16</sup> Among the most widely used methods in industry is the absorption of CO<sub>2</sub> using amine solutions, typically monoethanolamine

(MEA).<sup>18,19</sup> However, the energy-intensive process of regenerating the solvent after CO<sub>2</sub> capture makes this method fall short of the ambitious goal of achieving a CO<sub>2</sub> capture cost of \$20 per ton, as proposed by various research programs in the USA and Europe.<sup>16,20</sup> Reducing the costs of CO<sub>2</sub> capture is crucial for widespread implementation and to make it economically viable on a large scale.

One promising alternative for CO<sub>2</sub> capture and activation is the use of frustrated Lewis pairs (FLPs).<sup>21–23</sup> FLP systems, characterized by their inability to form traditional Lewis acid–Lewis base adducts, have shown the notable capability to activate stable molecules like CO<sub>2</sub>, N<sub>2</sub>, or H<sub>2</sub>.<sup>24–26</sup> Experimental and theoretical studies on the activation and sequestration of CO<sub>2</sub> by FLPs have been reported.<sup>27–32</sup>

Recently, a derivative of hexabenzocoronene, or hexa-cata-hexabenzocoronene, with N–B atoms in relative *para* positions has been synthesized<sup>33</sup> (Refcode: FEWKIE in CSD<sup>34</sup>). Nanographenes (NGs) and doped nanographenes have also been studied for their interaction with CO<sub>2</sub>, forming non-covalent complexes where the CO<sub>2</sub> molecule remains relatively unactivated.<sup>35–39</sup> In a recent theoretical study, it was suggested that a B<sub>3</sub>P<sub>3</sub>-doped NG could capture up to three CO<sub>2</sub> molecules, making it an attractive system for carbon dioxide capture<sup>32</sup> in agreement with other P/B FLPs reported in the literature.<sup>40–42</sup> However, the previous study only considered the influence of the Lewis base substitution. In this work, we focus on the effect of the Lewis acid substitution on the CO<sub>2</sub> capture. The reaction

<sup>a</sup> Instituto de Química Médica (CSIC), Juan de la Cierva, 3, E-28006 Madrid, Spain.  
E-mail: ibon@iqm.csic.es

<sup>b</sup> PhD Program in Theoretical Chemistry and Computational Modeling, Doctoral School, Universidad Autónoma de Madrid, 28049 Madrid, Spain

<sup>c</sup> Instituto de Química-Física Blas Cabrera (CSIC), Serrano, 119, E-28006 Madrid, Spain

† Electronic supplementary information (ESI) available. See DOI: <https://doi.org/10.1039/d4cp00496e>



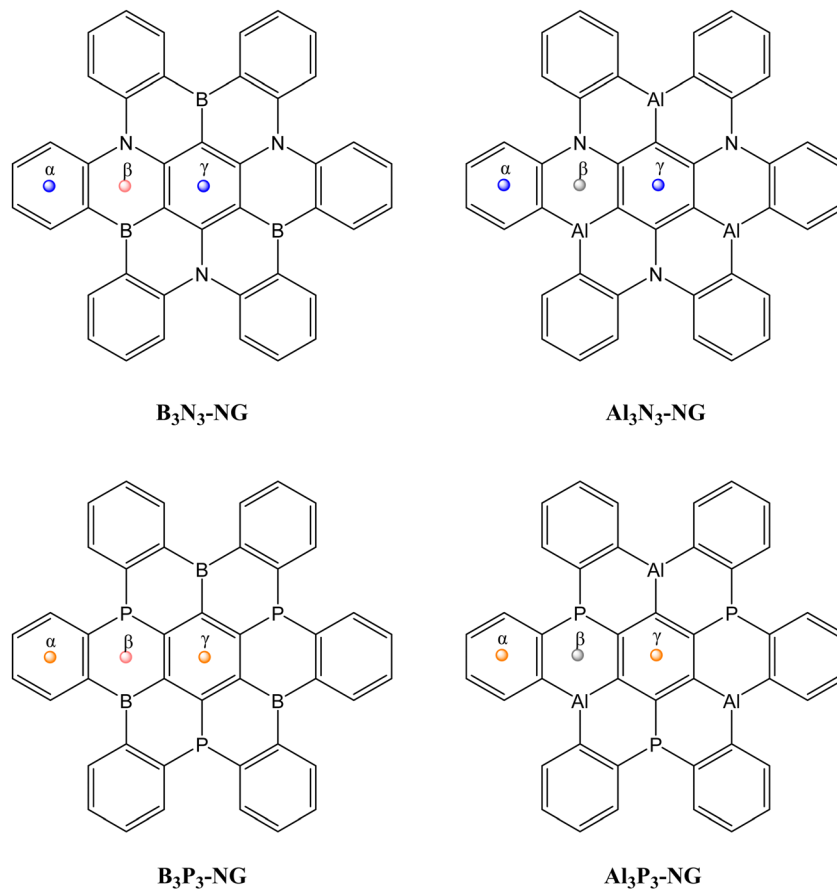


Fig. 1 Structure of the multi-FLP  $B_3N_3$ -NG,  $Al_3N_3$ -NG,  $B_3P_3$ -NG and  $Al_3P_3$ -NG used in this study. The centroids of the 6-member rings are indicated as  $\alpha$ ,  $\beta$ , and  $\gamma$ .

of four doped NGs, namely  $B_3N_3$ -NG,  $Al_3N_3$ -NG,  $B_3P_3$ -NG and  $Al_3P_3$ -NG (Fig. 1), with up to three  $CO_2$  molecules was investigated. Additionally, considering the growing interest in using charged FLPs<sup>43–45</sup> for  $CO_2$  reactions, the influence of a cation ( $Na^+$ ) interacting with the doped NG on the  $CO_2$  capture was also considered.

## Computational details

The structures under study, depicted in Fig. 1, were optimized with the scientific software Gaussian16<sup>46</sup> using the M06-2X DFT functional<sup>47</sup> and the 6-31+G(d) basis set.<sup>48</sup> The Berny optimization algorithm<sup>49</sup> and the synchronous transit-guided quasi-Newton (STQN) method<sup>50</sup> were used to locate the stationary points (energy minima and TSs, respectively). The optimized geometries were checked as energy minima (no imaginary frequency) or transition states (one imaginary frequency) by performing frequency calculations at the M06-2X/6-31+G(d) computational level. In order to obtain more accurate energies, single-point energy calculations were performed at the M06-2X/6-311++G(3df,3pd)<sup>51</sup> level of theory using the M06-2X/6-31+G(d) optimized geometries. This computational procedure gives similar results to the ones provided by the DLPNO-CCSD(T) computational level in the reaction of other FLPs with  $CO_2$ .<sup>52</sup>

The frequency calculations at the M06-2X/6-31+G(d) computational level were also used to obtain the enthalpy and entropy corrections.

The molecular electrostatic potential (MEP) was calculated in order to identify regions of favorable interaction with a positive point charge (negative regions of the MEP) and those with a negative charge (positive regions of the MEP). The MEP was calculated on the 0.001 a.u. electron density isosurface using the M06-2X/6-311++G(3df,3pd)//M06-2X/6-31+G(d) wavefunction and the Multiwfn software.<sup>53</sup>

The topological properties of the electron density were analyzed using the quantum theory of atoms in molecules (QTAIM)<sup>54,55</sup> as implemented in the AIMAll scientific software.<sup>56</sup> Electron density critical points (CPs), where the density gradient vanishes with respect to electron coordinates, were identified. These CPs are classified based on the number of non-zero eigenvalues (rank,  $w$ ) and the sum of the eigenvalue signs (signature,  $s$ ) as CP( $w,s$ ). Points of interest include attractor (3,−3), bond (3,−1), ring (3,+1), and cage critical points (3,+3). The covalent character of the interactions associated with bond critical points can be determined by examining the values of the electron density, Laplacian of the electron density, potential energy density, and kinetic energy density.<sup>57,58</sup> The molecular graphs were computed using the M06-2X/6-311++G(3df,3pd)//M06-2X/6-31+G(d) wavefunctions.



The natural bond orbital methodology,<sup>59</sup> as implemented in the NBO program (version 7.0),<sup>60</sup> was used to obtain a Lewis-like structure as regards to electron distribution of the systems and to compute the stabilization due to the charge transfer between occupied and empty orbitals.

The binding energy of the adducts ( $E_b$ ) was calculated as the difference between the adduct energy and the sum of the isolated monomers in their energy minimum configuration (eqn (1)). In order to quantify the cooperative effect when multiple molecules of  $\text{CO}_2$  interact with an NG, the total binding energy of the adducts was decomposed (eqn (2)) into deformation energy of the monomers ( $E_{\text{def}}$ ) (eqn (3)), two-body interaction energy [ $\Delta^2 E(ij)$ ] (eqn (4)), and a cooperative energy ( $C$ ). Here,  $E(i)$  represents the energy of the isolated monomer in its minimum energy state, and  $E'(i)$  represents the energy in the geometry of the supermolecule. This method is similar to the many-body energy analysis,<sup>61,62</sup> but it truncates the expansion in the two-body interaction term and includes the higher terms in the cooperativity component.

$$E_b = E(\text{adduct}) - E(\text{NG}) - n \times E(\text{CO}_2) \quad (1)$$

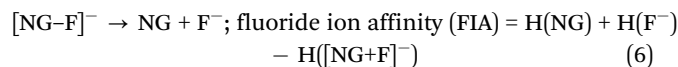
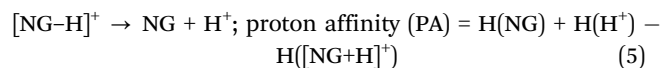
$$E_b = E_{\text{def}} + E_i + C = \sum E_{\text{def}}(i) + \sum \sum \Delta^2 E(ij) + C \quad (2)$$

$$E_{\text{def}}(i) = E(i) - E'(i) \quad (3)$$

$$\Delta^2 E(ij) = E(ij) - E'(i) - E'(j) \quad (4)$$

The basicity and acidity of the NG and adduct derivatives were evaluated based on their proton affinity (PA) and fluoride ion affinity (FIA),<sup>63–65</sup> respectively (eqn (5) and (6)). The enthalpies ( $H$ ) of the different compounds in eqn (5) (nanographene, NG, proton,  $\text{H}^+$ , and protonated nanographene,  $\text{NG-H}^+$ ) and eqn (6) (nanographene, NG, Fluoride,  $\text{F}^-$ , and their adduct,  $\text{NG-F}^-$ ) are used to calculate the PAs and FIAs. In order to obtain more accurate enthalpies, the electronic energy at the M06-2X/6-311++G(3df,3pd)//M06-2X/6-31+G(d) level was corrected with

the thermodynamic terms calculated at the M06-2X/6-31+G(d) level. As proven in previous papers,<sup>65–67</sup> these evaluations allow for a better understanding of the acidic and basic properties of the compounds and their interactions with  $\text{CO}_2$ .



The kinetics of the above reactions were obtained with the transition state theory,<sup>68</sup> and the rate constant of a given barrier was obtained by means of eqn (7).

$$k = \frac{k_b T}{h} e^{-\frac{\Delta G^\ddagger}{RT}} \quad (7)$$

where  $k$  is the rate constant in  $\text{s}^{-1}$ ,  $k_b$  is the Boltzmann constant,  $T$  is the temperature in Kelvin,  $h$  is the Planck constant,  $R$  is the gas constant and  $\Delta G^\ddagger$  is the free energy of activation.

## Results and discussion

We consider the sequential capture of up to three  $\text{CO}_2$  molecules on nanographene (NG) surfaces (Fig. 1). The capture of each  $\text{CO}_2$  molecule comprises the initial formation of a pre-reactive complex, which, after a transition state (TS), produces the adduct where the  $\text{CO}_2$  molecule forms covalent bonds between the oxygen atom and the Lewis acid atoms, as well as between the carbon atom in  $\text{CO}_2$  and the Lewis base atoms. The first step of these processes is shown in Fig. 2 with two examples.

This section has been divided into four subsections. First, we present the general properties of the four NG systems. Second, one  $\text{CO}_2$  molecule approached the NG systems and formed an adduct. The candidates considered as reactive toward  $\text{CO}_2$  will be further studied for multi- $\text{CO}_2$  capture.

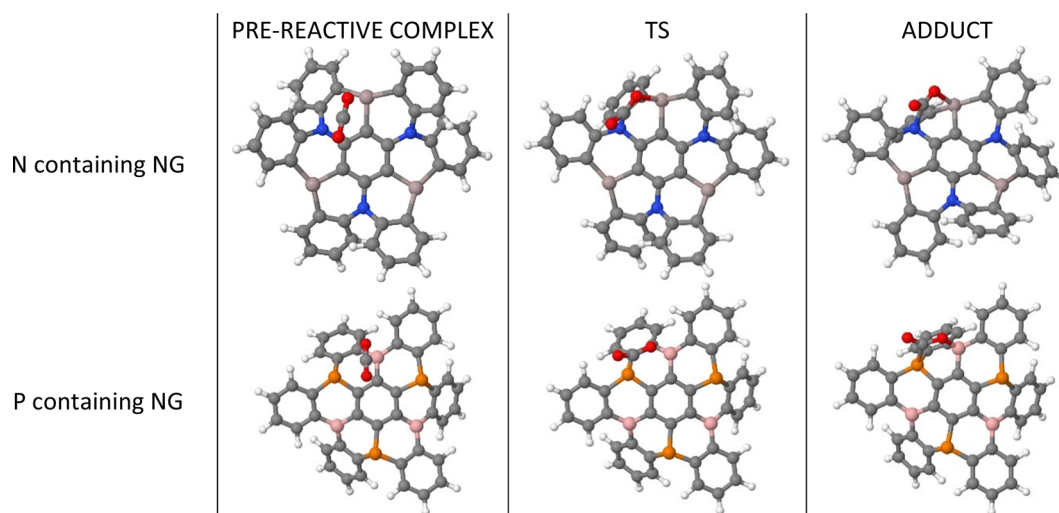


Fig. 2 Geometries of the stationary points for the first capture of  $\text{CO}_2$  by  $\text{Al}_3\text{N}_3$ -NG and  $\text{B}_3\text{P}_3$ -NG systems.



Finally, we analyze the effect of the presence of a  $\text{Na}^+$  cation, on both faces of the NG.

### Properties of isolated NGs

The potential reactivity of FLPs can be predicted by examining the acidity and basicity values of their molecular electrostatic potential (MEP). The four systems have  $C_3$  symmetry, *i.e.*, the LA/LB pairs are equivalent through a  $120^\circ$  rotation. Additionally, the nitrogen-containing NG species possess a planar environment around the nitrogen atoms, with both faces equivalent. Conversely, the NG species containing phosphorus do not have equivalent faces, but the most stable conformation has the lone pairs of the phosphorus atoms oriented in the same direction, making only one face reactive (see Fig. 3).

The geometry of  $\text{B}_3\text{N}_3\text{-NG}$  is available in the CSD database<sup>34</sup> (Refcode FEWKIE<sup>33</sup>), and our optimized geometry is in agreement with the experimental X-ray structure within an RMDS of 0.02 Å (Fig. S1, ESI†).

The geometries of the  $\text{B}_3\text{N}_3\text{-NG}$  and  $\text{Al}_3\text{N}_3\text{-NG}$  species are similar, with the lateral phenyl rings displaying similar orientations. The nitrogen atoms exhibit  $\text{sp}^2$  hybridization due to the delocalization of the lone pairs into the aromatic rings. NBO calculations reveal that the nitrogen atoms in the C–N bonds have an average hybridization of  $\text{sp}^{2.03}$  for  $\text{B}_3\text{N}_3\text{-NG}$  and  $\text{sp}^{2.08}$  for  $\text{Al}_3\text{N}_3\text{-NG}$ . Furthermore, the interaction between the nitrogen

lone pairs and the  $\pi$  antibonding orbitals stabilizes the system by approximately  $523.0 \text{ kJ mol}^{-1}$  and  $397.0 \text{ kJ mol}^{-1}$ , for  $\text{B}_3\text{N}_3\text{-NG}$  and  $\text{Al}_3\text{N}_3\text{-NG}$ , respectively. Regarding the MEP minima and maxima, the two systems show different features. The  $\text{B}_3\text{N}_3\text{-NG}$  systems have MEP maxima on boron atoms with values of  $-10.0 \text{ kJ mol}^{-1}$ , while the nitrogen atoms have MEP minima of  $-29.1 \text{ kJ mol}^{-1}$ . In contrast,  $\text{Al}_3\text{N}_3\text{-NG}$  shows three MEP maxima ( $+147.6 \text{ kJ mol}^{-1}$ ) on the aluminium atoms and three MEP minima on the nitrogen atom ( $-47.5 \text{ kJ mol}^{-1}$ ). The larger values of the MEP on the nitrogen atoms are in agreement with the NBO results, indicating that the nitrogen lone pairs in  $\text{B}_3\text{N}_3\text{-NG}$  are more delocalized than those in  $\text{Al}_3\text{N}_3\text{-NG}$ . Additionally, the larger acidity of aluminium compared to boron shows up, with boron atoms with MEP maxima of  $-10 \text{ kJ mol}^{-1}$ , while aluminium atoms have an MEP maximum value of  $+147.6 \text{ kJ mol}^{-1}$ . Based on this analysis, we can confirm that  $\text{Al}_3\text{N}_3\text{-NG}$  should be a better candidate for  $\text{CO}_2$  capture, as compared to  $\text{B}_3\text{N}_3\text{-NG}$ .

The phosphorus-containing NG species ( $\text{B}_3\text{P}_3\text{-NG}$  and  $\text{Al}_3\text{P}_3\text{-NG}$ ) exhibit a similar arrangement of MEP maxima and minima. The phosphorus atoms have an MEP negative minimum with values of  $-85.9$  and  $-93.7 \text{ kJ mol}^{-1}$  for the  $\text{B}_3\text{P}_3\text{-NG}$  and  $\text{Al}_3\text{P}_3\text{-NG}$  systems, respectively. The region close to boron atoms shows an MEP maximum of  $+29.9 \text{ kJ mol}^{-1}$  in the  $\text{B}_3\text{P}_3\text{-NG}$  molecule, whereas near aluminium atoms there is an MEP

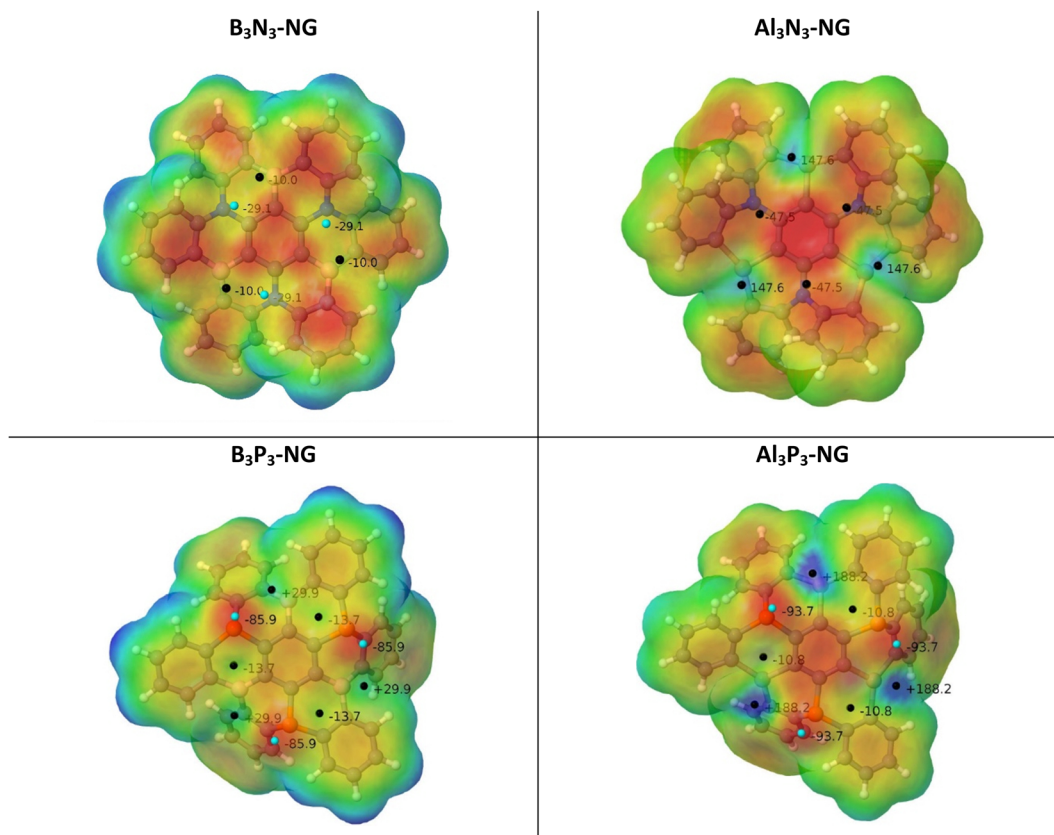


Fig. 3 MEP of the four NG systems. The location of the MEP maxima and minima is identified by black and cyan spheres and their values are indicated in  $\text{kJ mol}^{-1}$ .



**Table 1** Fluoride ion affinity and proton affinity in  $\text{kJ mol}^{-1}$  for the four monomers

System	$\text{B}_3\text{N}_3\text{-NG}$	$\text{Al}_3\text{N}_3\text{-NG}$	$\text{B}_3\text{P}_3\text{-NG}$	$\text{Al}_3\text{P}_3\text{-NG}$
FIA	295.8	435.6	354.6	450.2
PA	859.8	933.8	967.8	995.2

maximum of  $+188.2 \text{ kJ mol}^{-1}$  in the  $\text{Al}_3\text{P}_3\text{-NG}$  system. In the NG with phosphorus atoms, three FLP systems over six are deactivated by the presence of a negative MEP maximum, with  $-10.8 \text{ kJ mol}^{-1}$  and  $-13.7 \text{ kJ mol}^{-1}$  for  $\text{B}_3\text{P}_3\text{-NG}$  and  $\text{Al}_3\text{P}_3\text{-NG}$ , respectively. These MEP maxima are not found for the nitrogen-containing NGs ( $\text{B}_3\text{N}_3\text{-NG}$  and  $\text{Al}_3\text{N}_3\text{-NG}$ ). As previously reported,<sup>32</sup> this observation can be related to the angle between the  $\alpha$ ,  $\beta$ , and  $\gamma$  centroids of the 6-member rings (Fig. 1). In the case of  $\text{B}_3\text{N}_3\text{-NG}$  and  $\text{Al}_3\text{N}_3\text{-NG}$ , the  $\alpha$ - $\beta$ - $\gamma$  angles have values of  $162^\circ$  and  $155^\circ$ , respectively. As for  $\text{B}_3\text{P}_3\text{-NG}$ , the angles alternate between  $148^\circ$  and  $175^\circ$ . The same is observed for  $\text{Al}_3\text{P}_3\text{-NG}$ , but with an alternation from  $147^\circ$  to  $176^\circ$ . The most deactivated FLPs are those with the most planar angles ( $175^\circ$  and  $176^\circ$ ). Based on this analysis alone, we can infer that the  $\text{Al}_3\text{P}_3\text{-NG}$  system should be more reactive towards  $\text{CO}_2$  than  $\text{B}_3\text{P}_3\text{-NG}$ .

In order to evaluate the acidity and basicity of the boron/aluminium and nitrogen/phosphorus atom pairs, respectively, we computed the fluoride ion affinity (FIA) and the proton affinity (PA) (Table 1). The NG systems with Al exhibit higher FIA values compared to those with boron, in agreement with the reported values of the phenyl derivatives:  $\text{FIA}[\text{B}(\text{C}_6\text{H}_5)_3] = 320 \text{ kJ mol}^{-1}$  and  $\text{FIA}[\text{Al}(\text{C}_6\text{H}_5)_3] = 427 \text{ kJ mol}^{-1}$ .<sup>65</sup> As regards to

**Table 2** O–B/Al and C–N/P distances in Å. The angle on the  $\text{CO}_2$  molecule and the angle between the  $\alpha$ - $\beta$ - $\gamma$  centroids (Fig. 1) of the 6-member rings, all in degrees ( $^\circ$ ). The electron density at the BCP is given in a.u. and in parenthesis

	Geometry	Complex	TS	Adduct
$\text{B}_3\text{N}_3\text{-NG}$	B–O	3.11	1.66 (0.0885)	1.60 (0.1032)
	C–N	3.37	1.87 (0.1132)	1.73 (0.1527)
	O–C–O	179.2	141.2	135.7
	$\alpha$ - $\beta$ - $\gamma$	163.0	140.7	138.1
$\text{Al}_3\text{N}_3\text{-NG}$	Al–O	2.36 (0.0192)	1.93 (0.0571)	1.89 (0.0641)
	C–N	2.99	1.92 (0.1025)	1.75 (0.1476)
	O–C–O	177.9	143.1	136.6
	$\alpha$ - $\beta$ - $\gamma$	150.3	135.9	134.1
$\text{B}_3\text{P}_3\text{-NG}$	B–O	2.89	2.25 (0.0276)	1.58 (0.1134)
	C–P	3.33 (0.0085)	2.15 (0.0967)	1.90 (0.1599)
	O–C–O	178.9	144.4	129.8
	$\alpha$ - $\beta$ - $\gamma$	148.4	145.6	137.0
$\text{Al}_3\text{P}_3\text{-NG}$	Al–O	2.19 (0.0265)	2.07 (0.0366)	1.87 (0.0693)
	C–P	3.17 (0.0125)	2.74 (0.0314)	1.92 (0.1558)
	O–C–O	174.8	161.2	30.0
	$\alpha$ - $\beta$ - $\gamma$	143.9	142.3	141.6

basicity, the systems with P display higher basicities than those with N, in good agreement with the experimental PA values<sup>69</sup> of  $\text{N}(\text{C}_6\text{H}_5)_3$  ( $908.9 \text{ kJ mol}^{-1}$ ) and  $\text{P}(\text{C}_6\text{H}_5)_3$  ( $972.8 \text{ kJ mol}^{-1}$ ). The enhanced basicity of the P-NG systems as compared to N-NG can be attributed to the lower delocalization of the phosphorus lone pairs, leading to their higher availability as previously discussed. The trends in FIA and PA values are in agreement with the MEP values previously discussed (Fig. 3).

### First $\text{CO}_2$ capture

The stationary points of the first  $\text{CO}_2$  capture with two NGs are shown in Fig. 2. The energy and free energy profiles for the four NGs are displayed in Fig. 4 and Fig. S2 (ESI<sup>†</sup>), respectively. The  $\text{CO}_2$  adsorption on  $\text{B}_3\text{N}_3\text{-NG}$  is feasible and relatively stable, resulting in the formation of a complex with an energy of  $-18.5 \text{ kJ mol}^{-1}$ , as previously found.<sup>35,36</sup> However, the formation of a covalent adduct is unfavorable, as indicated by the positive and large relative energy ( $+132.0 \text{ kJ mol}^{-1}$ ). It can be anticipated that this adduct has a very low probability of existence, due to the small rate constant associated with the corresponding barrier ( $8.06 \times 10^{-20} \text{ s}^{-1}$ ).

The substitution of nitrogen by phosphorus ( $\text{B}_3\text{P}_3\text{-NG}$ ) does not significantly change the stability of the adsorption complex,  $-19.1$  for  $\text{B}_3\text{P}_3\text{-NG}$  vs.  $-18.5 \text{ kJ mol}^{-1}$  for  $\text{B}_3\text{N}_3\text{-NG}$ . However, the adduct is now slightly above the reactant energies ( $E_{\text{rel}} = -7.3 \text{ kJ mol}^{-1}$ ) and the TS is also stabilized (from  $137 \text{ kJ mol}^{-1}$  in  $\text{B}_3\text{N}_3\text{-NG}$  to  $42 \text{ kJ mol}^{-1}$  in  $\text{B}_3\text{P}_3\text{-NG}$ ), reducing the activation barrier. Although the adduct ( $E_{\text{rel}} = -7.3 \text{ kJ mol}^{-1}$ ) is below the complex, a rate constant of  $3.07 \times 10^2 \text{ s}^{-1}$  suggests that the reaction should take place.

The energetic profiles of  $\text{Al}_3\text{N}_3\text{-NG}$  and  $\text{B}_3\text{N}_3\text{-NG}$  share several similarities: a stable pre-reactive complex with stabilization energies of  $-19$  and  $-39 \text{ kJ mol}^{-1}$  respectively, TS and final product with positive relative energies and small energy difference between them (about  $5 \text{ kJ mol}^{-1}$ ). However, the replacement of B by Al decreases significantly the above energy values of the TS and final products.

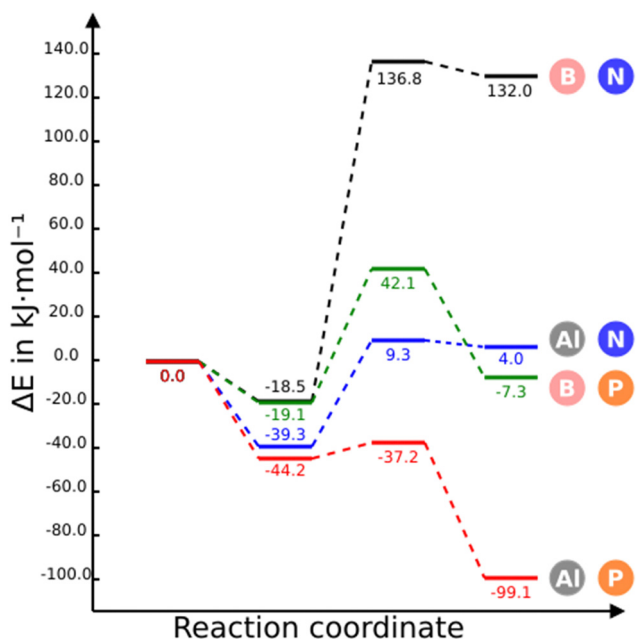


**Fig. 4** Energy profiles for the capture of one  $\text{CO}_2$  molecule by the  $\text{B}_3\text{N}_3\text{-NG}$ ,  $\text{B}_3\text{P}_3\text{-NG}$ ,  $\text{Al}_3\text{N}_3\text{-NG}$  and  $\text{Al}_3\text{P}_3\text{-NG}$  systems at M06-2X/6-311++G(3df,3dp)//M06-2X/6-31+G\* level of theory. The reference value ( $0.0 \text{ kJ mol}^{-1}$ ) corresponds to the sum of the energies of the isolated monomers in their energy minima configuration.



The substitution of nitrogen with phosphorus to form  $\text{Al}_3\text{P}_3\text{-NG}$  results in a highly reactive system towards  $\text{CO}_2$ . As shown in Fig. 4, all stationary points in this system are below the entrance channel. The reaction rate constant is considerably large ( $k = 1.01 \times 10^{11} \text{ s}^{-1}$ ), an indication that the  $\text{CO}_2$  capture by  $\text{Al}_3\text{P}_3\text{-NG}$  is both thermodynamically and kinetically favorable, making it the most promising candidate so far.

If the free energy at 298 K is considered (Fig. S2, ESI<sup>†</sup>) then only the  $\text{Al}_3\text{N}_3\text{-NG}$  and  $\text{Al}_3\text{P}_3\text{-NG}$  complexes are more stable than the entrance channel and the  $\text{Al}_3\text{P}_3\text{-NG-CO}_2$  is very stable ( $-52 \text{ kJ mol}^{-1}$ ). These results clearly indicate that the reaction is enthalpy driven.

Regarding the geometry of the stationary points and their electron density (Table 2), the higher stability of the aluminium-containing complexes can be attributed to the closer contact between aluminium and oxygen atoms compared to the B–O contact (3.11, 2.36, 2.88, and 2.18 Å for  $\text{B}_3\text{N}_3\text{-NG}$ ,  $\text{Al}_3\text{N}_3\text{-NG}$ ,  $\text{B}_3\text{P}_3\text{-NG}$  and  $\text{Al}_3\text{P}_3\text{-NG}$  respectively). In fact, when passing from boron to aluminium,  $\text{CO}_2$  undergoes a more significant bending in the complex ( $179.0^\circ$  to  $177.9^\circ$  in  $\text{B}_3\text{N}_3\text{-NG}$  and  $\text{Al}_3\text{N}_3\text{-NG}$ , respectively, and  $178.9^\circ$  to  $174.8^\circ$  in  $\text{B}_3\text{P}_3\text{-NG}$  and  $\text{Al}_3\text{P}_3\text{-NG}$ , respectively), and turns into a more activated molecule. Additionally, the AIM analysis reveals the presence of BCP between oxygen and aluminium in the complex of aluminium systems, whereas no BCP was found between boron and oxygen in the complexes with  $\text{B}_3\text{N}_3\text{-NG}$  and  $\text{B}_3\text{P}_3\text{-NG}$ . These results confirm Ashley *et al.*'s statement: "in Al-based FLP,  $\text{CO}_2$  activation proceeds by initial  $\text{Al} \cdots \text{O1}/4\text{C1}/4\text{O}$  interaction in a van der Waals complex, which

stands in contrast to other P/B examples where  $\text{CO}_2$  interacts with the Lewis base component first".<sup>22</sup>

The TSs and adduct geometries with the nitrogen-containing NG systems are very similar, with B/Al–O and N–C bonds formed by 96% and 92% in the TS of  $\text{B}_3\text{N}_3\text{-NG}$  and 97% and 91% in the case of the  $\text{Al}_3\text{N}_3\text{-NG}$  TS with respect to the bond length computed in the adducts. In contrast, the bond formations in the TSs for  $\text{B}_3\text{P}_3\text{-NG}$  are 70% and 88%, and 90% and 70% in  $\text{Al}_3\text{P}_3\text{-NG}$ . This indicates that in  $\text{B}_3\text{P}_3\text{-NG}$  FLPs, phosphorus attacks first, while in the case of  $\text{Al}_3\text{P}_3\text{-NG}$  FLPs, it is the aluminium atom that interacts first. This difference in bond formation is also reflected in the electron density at the BCPs, higher and closer to the final values in the nitrogen-containing systems compared to the phosphorus-containing NGs (Table 2). An excellent exponential correlation is found for the six BCPs obtained for the Al–O and C–P contacts *vs.* the interatomic distances (Fig. S3, ESI<sup>†</sup>), in agreement with previous reports.<sup>58,70,71</sup>

One possible reason for the difference in TS energies, aside from the differences in acidity and basicity, could be the deformation of the NG system and the bending of the lateral phenyl ring. The calculated deformation energy of the two monomers (NG plus  $\text{CO}_2$ ) in the TS accounts for 281, 194, 143 and 48  $\text{kJ mol}^{-1}$  for  $\text{B}_3\text{N}_3\text{-NG}$ ,  $\text{Al}_3\text{N}_3\text{-NG}$ ,  $\text{B}_3\text{P}_3\text{-NG}$  and  $\text{Al}_3\text{P}_3\text{-NG}$ , respectively. These results are in agreement with the difference between this angle on the three centroids  $\alpha$ ,  $\beta$ ,  $\gamma$  (Fig. 1) in the complex and this angle at the corresponding TS angle, with values of  $22.3^\circ$ ,  $14.4^\circ$ ,  $2.8^\circ$  and  $1.6^\circ$ , respectively.

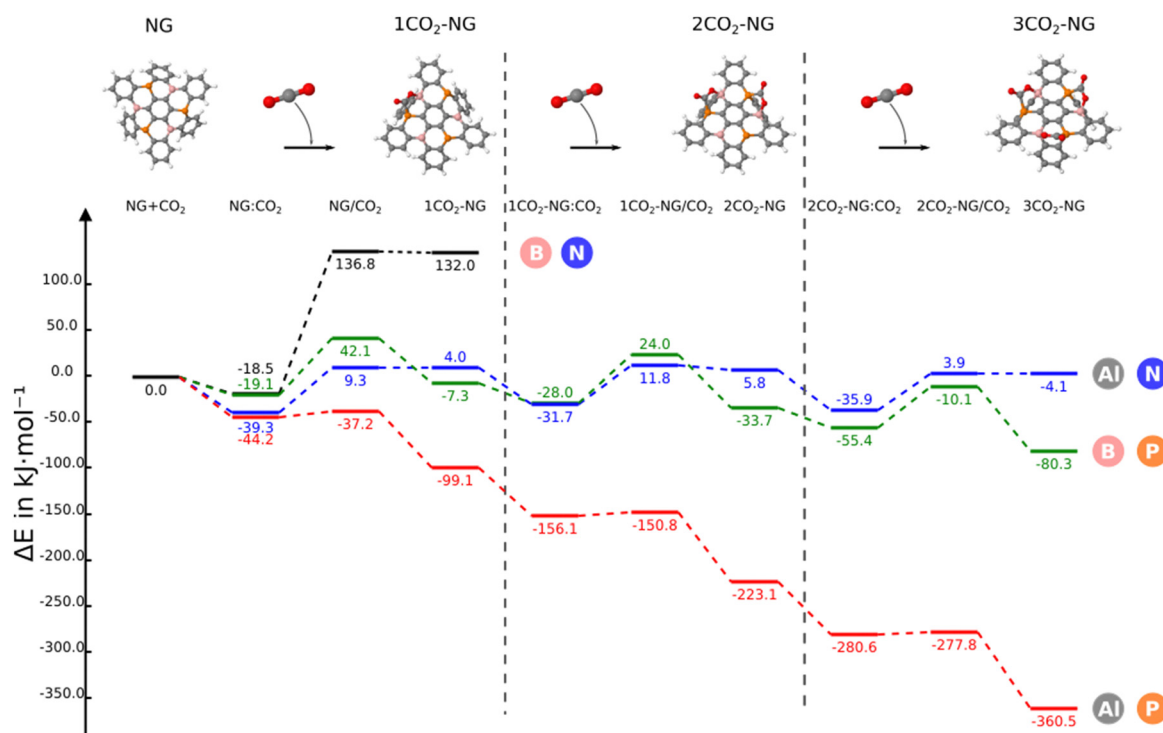


Fig. 5 Reaction profile of the different nanographenes with up to three  $\text{CO}_2$  molecules. The reference value ( $0.0 \text{ kJ mol}^{-1}$ ) corresponds to the sum of the energies of the isolated monomers in their energy minimum geometry.



### Multi capture

In this section, we consider the sequential reaction of the NG system with up to three CO<sub>2</sub> molecules. The B<sub>3</sub>N<sub>3</sub>-NG system is excluded from further studies since it is not able to form a stable adduct with CO<sub>2</sub>. Thus, this section only considers the B<sub>3</sub>P<sub>3</sub>-NG, Al<sub>3</sub>N<sub>3</sub>-NG and Al<sub>3</sub>P<sub>3</sub>-NG systems.

The reaction profiles are depicted in Fig. 5; as the number of interacting CO<sub>2</sub> molecules with Al<sub>3</sub>P<sub>3</sub>-NG increases, the systems become more stabilized. The energies of the different minima become more negative leading to the formation of an adduct with three CO<sub>2</sub> molecules and a relative energy of  $-360.5$  kJ mol<sup>-1</sup>.

A similar profile is observed for the reaction of B<sub>3</sub>P<sub>3</sub>-NG except for the first CO<sub>2</sub> addition where the complex is more stable than the adduct ( $-19.1$  vs.  $-7.3$  kJ mol<sup>-1</sup>, respectively), with the relative energy of the adduct with three CO<sub>2</sub> molecules being  $-80.3$  kJ mol<sup>-1</sup>. Finally, in Al<sub>3</sub>N<sub>3</sub>-NG, all complexes are more stable than the corresponding adducts, with no significant stabilization gain after the addition of three CO<sub>2</sub> molecules and a relative energy of the final product of  $-4.1$  kJ mol<sup>-1</sup>.

When the second capture occurs, a regioselectivity question arises in the TS when choosing between the remaining FLP sites. However, the product of the second CO<sub>2</sub> addition is the same, independently of the adduct formed in any of the two

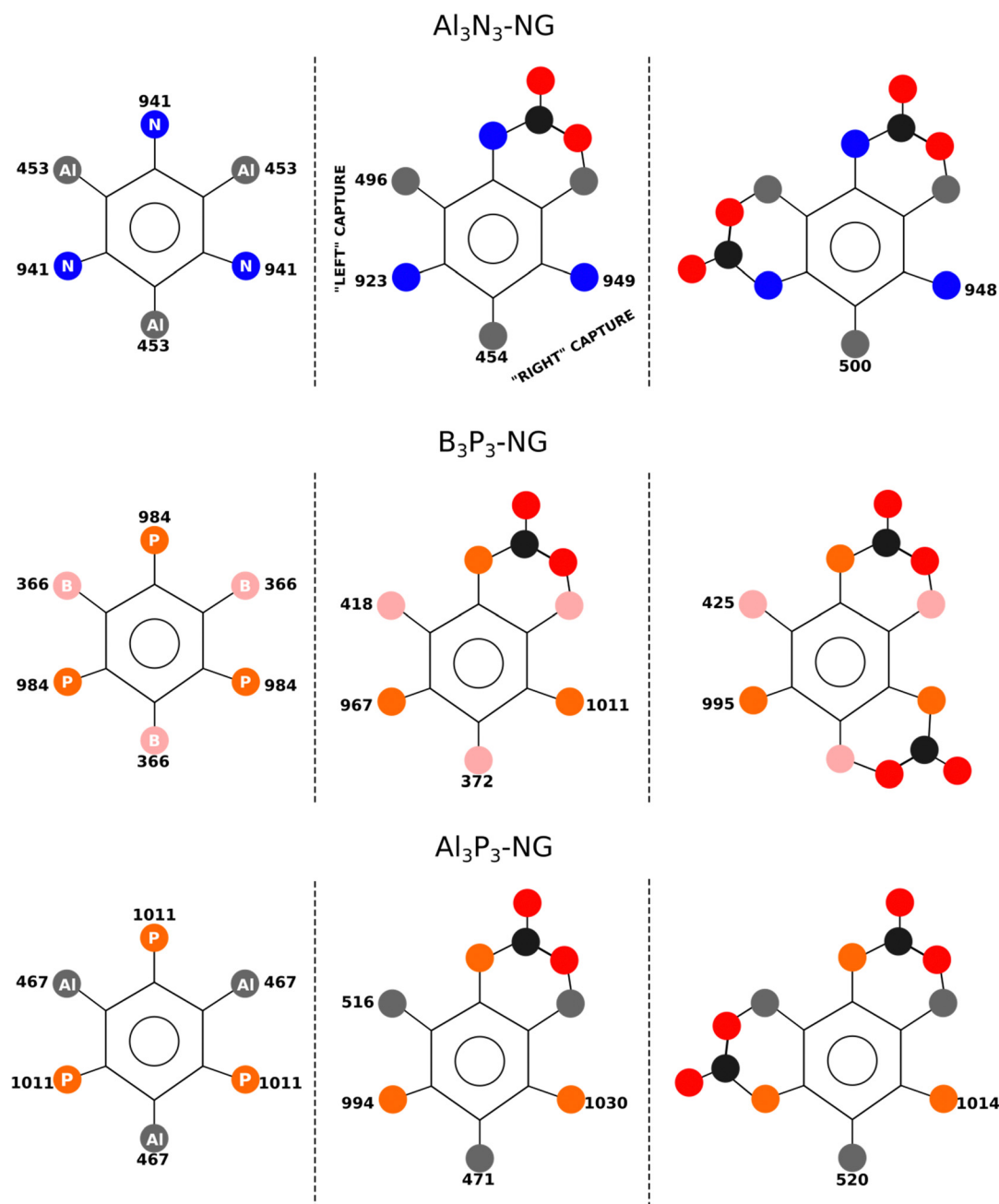


Fig. 6 FIA and PA of the different stationary points in kJ mol<sup>-1</sup>. The 2CO<sub>2</sub>-NG adduct associated with the lowest TS barrier is shown in the third column.



**Table 3** C–N and O–Al distances in the adducts (Å) and rate constant  $k$  ( $s^{-1}$ ) calculated with the Eyring eqn (7)

	NG-CO <sub>2</sub>	NG-(CO <sub>2</sub> ) <sub>2</sub>	NG-(CO <sub>2</sub> ) <sub>3</sub>
Al <sub>3</sub> N <sub>3</sub> -NG	$d(\text{C-N}) = 1.750$	1.744 <sup>a</sup>	1.750
	$d(\text{O-Al}) = 1.891$	1.879 <sup>a</sup>	1.849
	$k = 3.07 \times 10^2$	$2.18 \times 10^3$	$9.57 \times 10^3$
B <sub>3</sub> P <sub>3</sub> -NG	$d(\text{C-P}) = 1.900$	1.903 <sup>a</sup>	1.907
	$d(\text{O-B}) = 1.581$	1.570 <sup>a</sup>	1.560
	$k = 3.47$	$2.18 \times 10^2$	$2.41 \times 10^2$
Al <sub>3</sub> P <sub>3</sub> -NG	$d(\text{C-P}) = 1.920$	1.928 <sup>a</sup>	1.927
	$d(\text{O-Al}) = 1.868$	1.858 <sup>a</sup>	1.847
	$k = 5.93 \times 10^{10}$	$2.51 \times 10^{11}$	$3.79 \times 10^{11}$

<sup>a</sup> Average values of the two CO<sub>2</sub> molecules.

remaining FLP couples. The two TSs have been explored for the three NGs and only the most stable one (from 1 to 5 kJ mol<sup>-1</sup>) has been included in Fig. 5.

In the case of B<sub>3</sub>P<sub>3</sub>-NG, the fixation of the second CO<sub>2</sub> molecule on the right (see Fig. 6) enables a stabilization of the TS by 5 kJ mol<sup>-1</sup>, while the complexes have the same energies. Considering the reaction of Al<sub>3</sub>N<sub>3</sub>-NG and Al<sub>3</sub>P<sub>3</sub>-NG, the most favorable TS is the one that yields the adduct on the left (see Fig. 6). The complexes are more stable by 2 and 5 kJ mol<sup>-1</sup>, and the TSs are more stable by 1 and 3 kJ mol<sup>-1</sup> for Al<sub>3</sub>N<sub>3</sub>-NG and Al<sub>3</sub>P<sub>3</sub>-NG, respectively. The differences are not large, but they can still be at the origin of a certain kinetic regioselectivity. In order to gain insights into the regioselectivity of CO<sub>2</sub> fixation, the FIA and PA of the isolated NG and adducts are calculated and summarized in Fig. 6. The difference in the TS regioselectivity can be attributed to the fact that in Al/P or Al/N FLP systems, CO<sub>2</sub> initially forms a strong interaction with the aluminium atom. The FIA of these compounds determines which FLP is more likely to react. In the case of P/B NG, the interaction of the phosphorus with the carbon of CO<sub>2</sub> is more dominant, and consequently, the phosphorous with the highest PA will have the smallest activation barrier.

As regards the stability of the adduct and the TS, the relationship is not straightforward as their energies are correlated with both acidity and basicity. A linear correlation is obtained between the adduct energy and the FIA and the PA, with  $R^2 = 0.83$ , and a correlation with  $R^2 = 0.80$  for the TS, in both cases with  $n = 9$ . As previously mentioned, both FIA and PA contribute to stabilizing these stationary points.

**Table 4** Stabilization energy (kJ mol<sup>-1</sup>) of the NG systems upon formation of adducts with three CO<sub>2</sub> molecules in the presence of Na<sup>+</sup>. The corresponding cases without Na<sup>+</sup> are included for comparative purposes

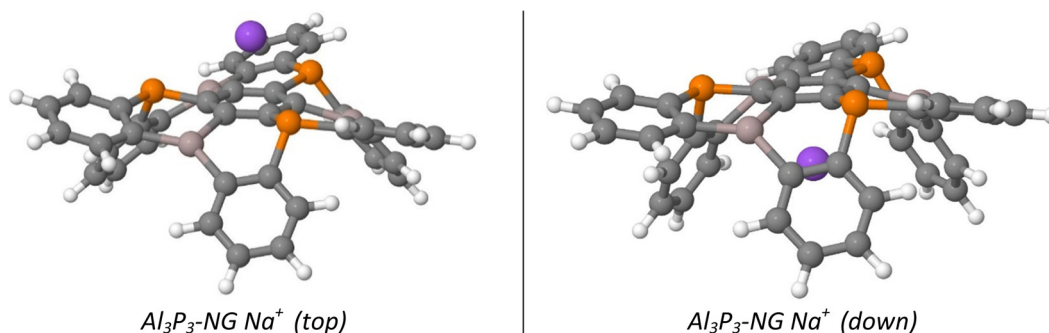
Na <sup>+</sup> disposition	B <sub>3</sub> N <sub>3</sub> -NG	Al <sub>3</sub> N <sub>3</sub> -NG	B <sub>3</sub> P <sub>3</sub> -NG	Al <sub>3</sub> P <sub>3</sub> -NG
Na <sup>+</sup> (top)	+258.4	-90.6	-167.0	-422.6
Na <sup>+</sup> (down)	+273.6	-21.8	-122.3	-379.3
—	Not found	-25.8	-107.2	-373.5

The energy terms obtained using the decomposition scheme from the methods section are gathered in Table S9 (ESI†). Depending on the NG systems studied, the relationship between the deformation energy and the absolute value of the two-body interaction energy is as follows: in the Al<sub>3</sub>N<sub>3</sub>-NG adducts, the deformation energy is larger than the two-body interaction energy; in the B<sub>3</sub>P<sub>3</sub>-NG systems, the deformation energy is slightly larger than the two-body interaction energy and, finally, in the Al<sub>3</sub>P<sub>3</sub>-NG adducts, the two-body interaction energy is clearly larger than those of the deformation energy. As regards to cooperativity effects, their values in the 2CO<sub>2</sub>-NG adducts are -5.8, -24.1 and -8.1 kJ mol<sup>-1</sup> for Al<sub>3</sub>N<sub>3</sub>-NG, B<sub>3</sub>P<sub>3</sub>-NG and Al<sub>3</sub>P<sub>3</sub>-NG, respectively, and the corresponding ones in the 3CO<sub>2</sub>-NG adducts are -21.6, -80.4 and -26.9 kJ mol<sup>-1</sup>, respectively. An analysis of the geometries of the LA–O and LB–C bonds (Table 3) in the addition products as a function of the number of CO<sub>2</sub> molecules shows that the LA–O distances decrease, an indication that these bonds become stronger with the number of CO<sub>2</sub> molecules attached. Otherwise, the LB–C contact remains unaltered or slightly elongated. Thus, the LA–O bond evolves in line with the energetic results obtained for the cooperativity effect in the adducts with two and three CO<sub>2</sub> molecules.

A systematic reduction in the reaction energy barriers is also observed in the Al<sub>3</sub>P<sub>3</sub>-NG system with the number of CO<sub>2</sub> molecules, which is also reflected in an increase in the reaction constant  $k$  (Table 3).

### CO<sub>2</sub> capture in the presence of Na<sup>+</sup>

In this subsection, we discuss the influence of a cation (Na<sup>+</sup>) in the capture of CO<sub>2</sub> molecules by NG systems. Two possible locations are considered for the cation (Fig. 7). In the first one (top), the cation interacts with the NG systems and the approaching CO<sub>2</sub> molecules. In the second approach (bottom),

**Fig. 7** Initial location of the Na<sup>+</sup> cation in the NG systems.

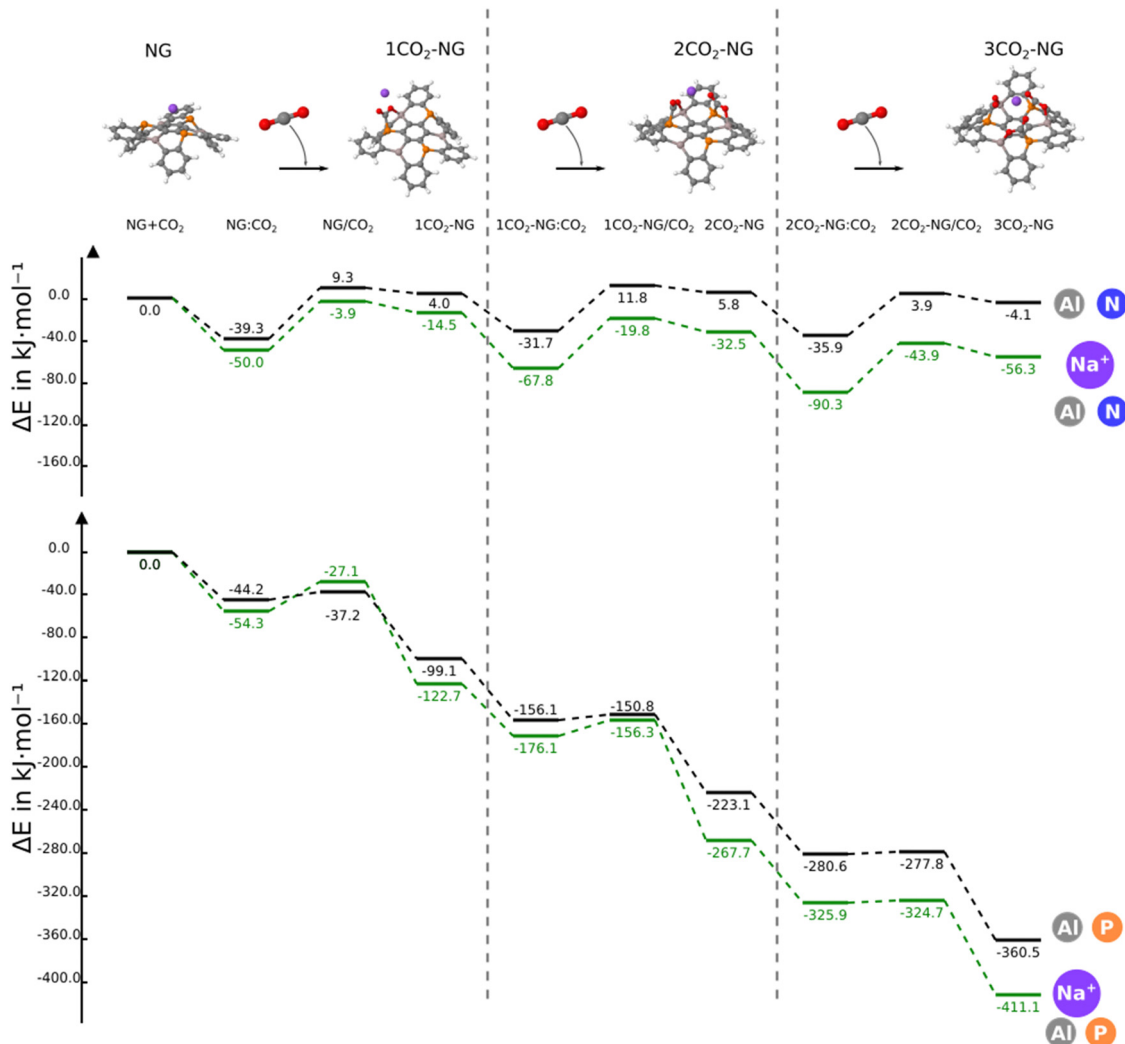


Fig. 8 Comparative energy profiles for the reaction of  $\text{Al}_3\text{N}_3\text{-NG}$  and  $\text{Al}_3\text{P}_3\text{-NG}$  in the absence/presence of  $\text{Na}^+$  with three  $\text{CO}_2$  molecules.

the cation interacts with the NG system only, whereas the  $\text{CO}_2$  molecules interact with the NG on its opposite face.

The interaction energy of the cation with the isolated NGs on the two sides is the same for the  $\text{B}_3\text{N}_3\text{-NG}$  ( $-167 \text{ kJ mol}^{-1}$ ) and  $\text{Al}_3\text{N}_3\text{-NG}$  ( $-200 \text{ kJ mol}^{-1}$ ), whereas in the  $\text{B}_3\text{P}_3\text{-NG}$ , the down complex is more stable (*top*,  $-175$  and *down*,  $-183 \text{ kJ mol}^{-1}$ ) and in  $\text{Al}_3\text{P}_3\text{-NG}$  is the opposite with the *top* complex being more stable ( $-194$  and  $-185 \text{ kJ mol}^{-1}$ ). The complex formation does not change the geometry of the NG in the nitrogen-containing NG ( $\text{B}_3\text{N}_3\text{-NG}$  and  $\text{Al}_3\text{N}_3\text{-NG}$ ). In contrast, in the phosphorous NG, the deformation of the system is responsible for their stability (Fig. S4, ESI<sup>†</sup>).

The two possible adducts of three  $\text{CO}_2$  molecules approaching the NG in the presence of  $\text{Na}^+$  have been explored. Their stability is listed in Table 4. In the  $\text{B}_3\text{N}_3\text{-NG}$ , it is possible to locate the adducts in the presence of  $\text{Na}^+$  which are absent without the cation, but with very high relative energy as an indication of their instability. In the other three NG systems, the adducts with  $\text{Na}^+$  in *down* orientation give stabilization energies which are very similar to those without the cation. In

contrast, a significant stabilization takes place if the  $\text{Na}^+$  cation is located in *top* orientation/location.

We now discuss the reaction to yield the adducts with the  $\text{Na}^+$  in the *top* arrangement, with those with the  $\text{Na}^+$  in the *down* orientation included in the ESI.<sup>†</sup>

The energy profile for the addition of three  $\text{CO}_2$  molecules in the presence of the  $\text{Na}^+$  cation shows three stationary points per added  $\text{CO}_2$  molecule: non-covalent complex, adduct and TS connecting them (Fig. 8). Only in the NG system with boron, additional stationary points are found due to the  $\text{Na}^+\text{-OCO}$  interactions in analogy to those found for the pentacene/ $\text{K}^+$  system (Fig. S5, ESI<sup>†</sup>).<sup>32,52</sup> The comparison of the energy profiles with and without  $\text{Na}^+$  in the same NG system shows that the presence of the cation reduces the relative energy of the stationary points with the exception of TS1 of  $\text{Al}_3\text{P}_3\text{-NG}$ ,  $10 \text{ kJ mol}^{-1}$  less stable in the presence of the cation.

An interesting effect due to the presence of the cation is the activation of the  $\text{CO}_2$  molecule even before the adduct. In addition, the TSs show that the LB-C bond is more advanced in all cases than the LA-O.



The adduct formation modifies the geometries and the electronic distribution of the NGs and CO<sub>2</sub> molecules. Thus, a significant dipole moment enhancement is observed in the adducts up to 6.2 and 6.3 Debyes for the Al<sub>3</sub>P<sub>3</sub>-NG-(CO<sub>2</sub>)<sub>2</sub> and Al<sub>3</sub>P<sub>3</sub>-NG-(CO<sub>2</sub>)<sub>3</sub> adducts, respectively. This effect is mostly due to the distortion in the CO<sub>2</sub> molecules that contribute around 1.3 Debye per molecule. This polarity increase should favor adducts *vs.* complex in polar environments.<sup>15,30,72</sup>

## Conclusions

The electronic structure computations carried out in this work with doped nanographenes (NGs) with up to three CO<sub>2</sub> molecules, with and without the presence of a sodium cation, can be summarised as follows:

- In the case of NG systems containing aluminium as a LA, the CO<sub>2</sub> molecule first interacts with the LA. In contrast, in NGs based on boron, the LB is the first to attack CO<sub>2</sub>.

- The LB species is directly involved in the general shape of the reaction profile. Due to  $\pi$ -electron delocalization, the NG systems containing nitrogen form non-stable adducts that evolve back to the complex.

- The nitrogen-containing NG systems tend to exhibit larger deformation energy and, consequently, larger activation energies due to the delocalization of the nitrogen lone pairs. These NGs also tend to have TSs close to the adducts. Conversely, the Al<sub>3</sub>P<sub>3</sub>-NG systems are highly reactive towards CO<sub>2</sub> and exhibit the TS close to the pre-reactive complexes.

- The FIA and PA of atoms involved in the first reactions determine the kinetic regioselectivity of the studied multi-FLPs. In NG systems with aluminium, CO<sub>2</sub> reacts with the more acidic free aluminium, while in the other NG cases, the CO<sub>2</sub> molecule reacts with the more basic LB.

- There is a cooperative effect in Al<sub>3</sub>N<sub>3</sub>-NG and Al<sub>3</sub>P<sub>3</sub>-NG systems in the third CO<sub>2</sub> capture, and in B<sub>3</sub>P<sub>3</sub>-NG in the second and third capture. The cooperativity can be attributed to shrinkage of the LA-O bonds.

- B<sub>3</sub>P<sub>3</sub>-NG and Al<sub>3</sub>P<sub>3</sub>-NG exhibit interesting properties for the capture of up to three CO<sub>2</sub> molecules, indicating their potential as promising candidates for CO<sub>2</sub> sequestration.

The presence of a cation on the same side where the adduct formation takes place stabilizes these adducts by activating the electrophilicity of the CO<sub>2</sub> non-covalent complex and interacting with the highly polar CO<sub>2</sub> molecule in the adducts.

These findings provide valuable insights into the reactivity and regioselectivity of doped nanographenes with CO<sub>2</sub> fixation and highlight the impact of LAs and LBs in driving the reactions. Finally, we should emphasize that the combination of Al and P atoms seems to be the most suitable for the activation/sequestration of CO<sub>2</sub> in doped nanographenes.

## Conflicts of interest

There are no conflicts to declare.

## Acknowledgements

This work was carried out with financial support from the Ministerio de Ciencia, Innovación y Universidades (Project PID2021-125207NB-C32). We are also grateful to the Centro de Supercomputación de Galicia (CESGA), CTI (CSIC) and the Irish Centre for High-End Computing (ICHEC, Dublin) for their continued computational support.

## References

- 1 P. Nejat, F. Jomehzadeh, M. M. Taheri, M. Gohari and M. Z. Abd. Majid, *Renew. Sust. Energ. Rev.*, 2015, **43**, 843–862.
- 2 A. Kijewska and A. Bluszczyk, *J. Sustain. Min.*, 2016, **15**, 133–142.
- 3 J. Xu, M. Zhou and H. Li, *Resour., Conserv. Recycl.*, 2018, **129**, 326–332.
- 4 N. Kuhn, M. Steimann and G. Weyers, *Z. Naturforsch. B*, 1999, **54**, 427–433.
- 5 H. A. Duong, T. N. Tekavec, A. M. Arif and J. Louie, *Chem. Commun.*, 2004, 112–113.
- 6 Y. Kayaki, M. Yamamoto and T. Ikariya, *Angew. Chem., Int. Ed.*, 2009, **48**, 4194–4197.
- 7 S. Wang and X. Wang, *Angew. Chem., Int. Ed.*, 2016, **55**, 2308–2320.
- 8 I. Alkorta, M. M. Montero-Campillo and J. Elguero, *Chem. – Eur. J.*, 2017, **23**, 10604–10609.
- 9 M. M. Montero-Campillo, I. Alkorta and J. Elguero, *Phys. Chem. Chem. Phys.*, 2018, **20**, 19552–19559.
- 10 C. Villiers, J.-P. Dognon, R. Pollet, P. Thuéry and M. Ephritikhine, *Angew. Chem., Int. Ed.*, 2010, **49**, 3465–3468.
- 11 S. Anila and C. H. Suresh, *Phys. Chem. Chem. Phys.*, 2021, **23**, 13662–13671.
- 12 F. Buß, P. Mehlmann, C. Mück-Lichtenfeld, K. Bergander and F. Dielmann, *J. Am. Chem. Soc.*, 2016, **138**, 1840–1843.
- 13 P. Mehlmann, C. Mück-Lichtenfeld, T. T. Y. Tan and F. Dielmann, *Chem. – Eur. J.*, 2017, **23**, 5929–5933.
- 14 I. Alkorta, C. Trujillo, G. Sánchez-Sanz and J. Elguero, *Inorganics*, 2018, **6**, 110.
- 15 G. Sánchez-Sanz, I. Alkorta, J. Elguero and C. Trujillo, *Chem. Phys. Chem.*, 2019, **20**, 3195–3200.
- 16 R. J. Krupadam and S. S. Rayalu, *Emergent Mater.*, 2021, **4**, 545–563.
- 17 J. A. Rudd, *Nat. Chem.*, 2022, **14**, 360.
- 18 S. Freguia and G. T. Rochelle, *AIChE J.*, 2003, **49**, 1676–1686.
- 19 P. Luis, *Desalination*, 2016, **380**, 93–99.
- 20 F. d'Amore and F. Bezzo, *Int. J. Greenhouse Gas Control*, 2017, **65**, 99–116.
- 21 E. Gerhard and W. S. Douglas, *Frustrated Lewis Pairs I*, Springer, Berlin, Heidelberg, 2013.
- 22 E. Gerhard and W. S. Douglas, *Frustrated Lewis Pairs II*, Springer, Berlin, Heidelberg, 2013.
- 23 J. C. Slootweg and A. R. Jupp, *Frustrated Lewis Pairs*, Springer Chem, 2020.
- 24 A. L. Travis, S. C. Binding, H. Zaher, T. A. Q. Arnold, J.-C. Buffet and D. O'Hare, *Dalton Trans.*, 2013, **42**, 2431–2437.



- 25 G. Kehr and G. Erker, *Chem. Rec.*, 2017, **17**, 803–815.
- 26 R. Pal, M. Ghara and P. K. Chattaraj, *Catalysts*, 2022, **12**, 201.
- 27 N. Von Wolff, G. Lefèvre, J.-C. Berthet, P. Thuéry and T. Cantat, *ACS Catal.*, 2016, **6**, 4526–4535.
- 28 D. Zhuang, A. M. Rouf, Y. Li, C. Dai and J. Zhu, *Chem. – Asian J.*, 2020, **15**, 266–272.
- 29 G. Sharma, P. D. Newman and J. A. Platts, *J. Mol. Graphics Modell.*, 2021, **105**, 107846.
- 30 M. Ferrer, I. Alkorta, J. Elguero and J. M. Oliva-Enrich, *J. Phys. Chem. A*, 2021, **125**, 6976–6984.
- 31 S. Soroudi and M. Z. Kassaei, *J. Phys. Org. Chem.*, 2022, **35**.
- 32 M. Ferrer, I. Alkorta, J. Elguero and J. M. Oliva-Enrich, *Sci. Rep.*, 2023, **13**, 2407.
- 33 K. Matsui, S. Oda, K. Yoshiura, K. Nakajima, N. Yasuda and T. Hatakeyama, *J. Am. Chem. Soc.*, 2018, **140**, 1195–1198.
- 34 C. R. Groom, I. J. Bruno, M. P. Lightfoot and S. C. Ward, *Acta Crystallogr., Sect. B*, 2016, **72**, 171–179.
- 35 R. Balasubramanian and S. Chowdhury, *J. Mater. Chem. A*, 2015, **3**, 21968–21989.
- 36 D. Saha, K. Nelson, J. Chen, Y. Lu and S. Ozcan, *J. Chem. Eng. Data*, 2015, **60**, 2636–2645.
- 37 A. A. Salari, *C. R. Chim*, 2017, **20**, 758–764.
- 38 V. Babar, S. Sharma and U. Schwingenschlögl, *J. Phys. Chem. C*, 2020, **124**, 5853–5860.
- 39 G. Wang, J. Yu, K. Zheng, Y. Huang, X. Li, X. Chen and L. Q. Tao, *IEEE Electron Device Lett.*, 2020, **41**, 1404–1407.
- 40 C. Appelt, H. Westenberg, F. Bertini, A. W. Ehlers, J. C. Slootweg, K. Lammertsma and W. Uhl, *Angew. Chem., Int. Ed.*, 2011, **50**, 3925–3928.
- 41 G. Ménard and D. W. Stephan, *Angew. Chem., Int. Ed.*, 2011, **50**, 8396–8399.
- 42 P. Federmann, R. Müller, F. Beckmann, C. Lau, B. Cula, M. Kaupp and C. Limberg, *Chem. – Eur. J.*, 2022, **28**, e2022004.
- 43 E. Von Grotthuss, S. E. Prey, M. Bolte, H.-W. Lerner and M. Wagner, *Angew. Chem., Int. Ed.*, 2018, **57**, 16491–16495.
- 44 S. E. Prey and M. Wagner, *Adv. Synth. Catal.*, 2021, **363**, 2290–2309.
- 45 J. E. Barker, A. D. Obi, D. A. Dickie and R. J. Gilliard, Jr., *J. Am. Chem. Soc.*, 2023, **145**, 2028–2034.
- 46 M. J. Frisch, G. W. Trucks, H. B. Schlegel, G. E. Scuseria, M. A. Robb, J. R. Cheeseman, G. Scalmani, V. Barone, G. A. Petersson, H. Nakatsuji, X. Li, M. Caricato, A. V. Marenich, J. Bloino, B. G. Janesko, R. Gomperts, B. Mennucci, H. P. Hratchian, J. V. Ortiz, A. F. Izmaylov, J. L. Sonnenberg Williams, F. Ding, F. Lipparini, F. Egidi, J. Goings, B. Peng, A. Petrone, T. Henderson, D. Ranasinghe, V. G. Zakrzewski, J. Gao, N. Rega, G. Zheng, W. Liang, M. Hada, M. Ehara, K. Toyota, R. Fukuda, J. Hasegawa, M. Ishida, T. Nakajima, Y. Honda, O. Kitao, H. Nakai, T. Vreven, K. Throssell, J. A. Montgomery Jr., J. E. Peralta, F. Ogliaro, M. J. Bearpark, J. J. Heyd, E. N. Brothers, K. N. Kudin, V. N. Staroverov, T. A. Keith, R. Kobayashi, J. Normand, K. Raghavachari, A. P. Rendell, J. C. Burant, S. S. Iyengar, J. Tomasi, M. Cossi, J. M. Millam, M. Klene, C. Adamo, R. Cammi, J. W. Ochterski, R. L. Martin, K. Morokuma, O. Farkas, J. B. Foresman and D. J. Fox, *Gaussian 16; Revision, A.03*, Gaussian, Inc., Wallingford, CT, USA, 2016.
- 47 Y. Zhao and D. G. Truhlar, *Theor. Chem. Acc.*, 2008, **120**, 215–241.
- 48 M. J. Frisch, J. A. Pople and J. S. Binkley, *J. Chem. Phys.*, 1984, **80**, 3265–3269.
- 49 H. B. Schlegel, *J. Comput. Chem.*, 1982, **3**, 214–218.
- 50 C. Peng, P. Y. Ayala, H. B. Schlegel and M. J. Frisch, *J. Comput. Chem.*, 1996, **17**, 49–56.
- 51 P. C. Hariharan and J. A. Pople, *Theor. Chim. Acta*, 1973, **28**, 213–222.
- 52 M. Ferrer, I. Alkorta, J. Elguero and J. M. Oliva-Enrich, *Phys. Chem. Chem. Phys.*, 2023, **25**, 22512–22522.
- 53 T. Lu and F. Chen, *J. Comput. Chem.*, 2012, **33**, 580–592.
- 54 R. F. W. Bader, *Acc. Chem. Res.*, 1985, **18**, 9–15.
- 55 P. L. A. Popelier, F. M. Aicken and S. E. O'Brien, in *Chemical Modelling: Applications and Theory*, ed. A. Hinchliffe, The Royal Society of Chemistry, 2000, vol. 1, pp. 143–198.
- 56 T. A. Keith, *AIMAll*, 19.10.12 Version ([aim.tkgristmill.com](http://aim.tkgristmill.com)), 2019.
- 57 I. Rozas, I. Alkorta and J. Elguero, *J. Am. Chem. Soc.*, 2000, **122**, 11154–11161.
- 58 E. Espinosa, I. Alkorta, J. Elguero and E. Molins, *J. Chem. Phys.*, 2002, **117**, 5529–5542.
- 59 F. Weinhold and C. R. Landis, *Valency and Bonding: A Natural Bond Orbital Donor-Acceptor Perspective*, Cambridge University Press, Cambridge, 2005.
- 60 E. D. Glendening, C. R. Landis and F. Weinhold, *J. Comput. Chem.*, 2019, **40**, 2234–2241.
- 61 S. S. Xantheas, *J. Chem. Phys.*, 1994, **100**, 7523–7534.
- 62 D. Hankins, J. W. Moskowitz and F. H. Stillinger, *J. Chem. Phys.*, 2003, **53**, 4544–4554.
- 63 A. K. Chandra and A. Goursot, *J. Phys. Chem.*, 1996, **100**, 11596–11599.
- 64 I. B. Sivaev and V. I. Bregadze, *Coord. Chem. Rev.*, 2014, **270–271**, 75–88.
- 65 P. Erdmann, J. Leitner, J. Schwarz and L. Greb, *Chem. Phys. Chem.*, 2020, **21**, 987–994.
- 66 Z. Wang, F. Wang, X.-S. Xue and P. Ji, *Org. Lett.*, 2018, **20**, 6041–6045.
- 67 M. Ferrer, I. Alkorta, J. Elguero and J. M. Oliva-Enrich, *ChemPhysChem*, 2022, **23**, e202200204.
- 68 H. Eyring, *J. Chem. Phys.*, 1935, **3**, 107–115.
- 69 *NIST Chemistry WebBook*, 2023.
- 70 G. Sánchez-Sanz, I. Alkorta and J. Elguero, *Mol. Phys.*, 2011, **109**, 2543–2552.
- 71 I. Alkorta, M. Solimannejad, P. Provasi and J. Elguero, *J. Phys. Chem. A*, 2007, **111**, 7154–7161.
- 72 M. Ferrer, I. Alkorta and J. Elguero, *Struct. Chem.*, 2024, **35**, 393–405.

